Supplementary Information

Intercalation of I^- and Cl^- anions into fluorinated graphite positive electrode for halogen-based dual-ion battery

Yueyuan Xu[a], Dongdong Lv[b], Wei Sun[a,b], Hongyu Wang[c] and Yuhao Huang*[,a,b]

[a]Key Laboratory of Laser Technology and Optoelectronic Functional Materials of Hainan Province, Key Laboratory of Functional Materials and Photoelectrochemistry of Haikou, College of Chemistry and Chemical Engineering, Hainan Normal University, Haikou 571158, China

[b] Hainan Engineering Research Centre of Tropical Ocean Advanced Optoelectronic Functional Materials, Hainan Normal University, Haikou 571158, China

[c] Key Laboratory of UV-Emitting Materials and Technology, Northeast Normal University, Changchun 130024, China

*Corresponding author: yhhuang1993@163.com (Dr. Y. H. Huang)

Methods

Materials. Fluorinated graphite ($CF_{0.56}$, 128.61 m^2 g^{-1}), zinc iodide (AR, ≥98% ZnI_2), and zinc chloride (99% $ZnCl_2$) were purchased from Shanghai Macklin Biochemical Co., Ltd. Carboxymethyl cellulose (CMC) and glass fiber filter paper (GA-100) were obtained from Hefei Kejing Material Technology Co., Ltd. Natural graphite (NG, 7.94 m^2 g^{-1}), conductive agent (Super P), titanium foil (>99.9%, thickness: 0.01 mm), titanium mesh (50 mesh) and zinc foil (>99.9%, thickness: 0.1 mm) were purchased from Kelude Co., Ltd.

Cell Assembly. Active material (NG or $CF_{0.56}$,), conductive agent (Super P), and binder (CMC) in a weight ratio of 8:1:1 was weighed into a beaker. An appropriate amount of ultrapure water was added and mixed uniformly to form a homogeneous electrode slurry. The resulting slurry was then coated onto titanium foil and uniformly spread using a blade with a gap of 30~40 μm. The coated foil was transferred to a 50°C oven and dried for 12 h. After drying, the electrode was cut into disks with a diameter of 14 mm using a manual punching machine (coating thickness: 40~60 μm; active mass loading: 3~6 mg). Two-electrode cells were assembled using NG or $CF_{0.56}$ as the positive electorde, Zn foil as the negative electrode, and two pieces of glass fiber separator (diameter: 16 mm) soaked by 280 μL of electrolyte (3 m (mol kg^{-1}) ZnI_2 + 27 m $ZnCl_2$).

Electrochemical Measurements. Galvanostatic charge-discharge (GCD) tests were performed at a current density of 0.75 A g^{-1} using two-electrode cells by battery testing system (CT3001A, Wuhan Land Electronics Co., Ltd.). Cyclic voltammetry (CV, voltage range: 0.5~2.0 V vs. Zn/Zn^{2+}, scan rate: 0.5 mV s^{-1}) and electrochemical impedance spectroscopy (EIS, frequency range: 0.01~10^5 Hz, amplitude: 5 mV) were conducted using a three-electrode setup (Zn foil served as the reference electrode) on an electrochemical workstation (DH7006, Donghua Technologies Co., Ltd.). Based on the Warburg impedance, the diffusion coefficient *(D_{anion})* of the I^- and Cl^- anions within solid electrode were calculated by this equation: $\sigma = \frac{V_m}{nFA\sqrt{2}\sqrt{D_{anion}}}\left(\frac{dE}{dQ}\right)$, where V_m is

the molar volume of the active material calculated by tap densities, $\frac{dE}{dQ}$ is the slope of the potential *(E)* against the amount of charge *(Q)* at the electrode calculated by the CV curve, *F* is the Faraday constant, *A* is the electrode area, and *n* is the number of charge transfer. The σ is the Warburg coefficient derived from the low-frequency region of EIS spectra by this equation: $Z_w = \sigma\omega^{-\frac{1}{2}}(1-j)$, where ω is the angular frequency, and *j* is the imaginary unit.

Others: X-ray diffraction (XRD) measurements were performed on a Rigaku Ultima IV diffractometer at a scanning rate of 10° min^{-1} within the 2θ range of 10–60°. Scanning electron microscopy (SEM) images were obtained with a Zeiss Sigma 500 field-emission SEM (Germany).

***In-situ* Electrochemical Characterizations.** *In-situ* Raman spectroscopy was carried out using a RENISHAW inVia Raman Microscope. *In-situ* optical images of the battery were captured using a metallographic microscope (Shanghai Wumo Optical Instrument Co., Ltd.). Electrochemical quartz crystal microbalance (EQCM) was performed on quartz plate with Pt coating (intrinsic frequency: 5 MHz, diameter: 14 mm, active mass loading: ~70 μg cm^{-2}) by QCM-D (Biolin Scientific) under 50°C (for the liquidity of electrolyte).

Unless otherwise mentioned, Swagelok battery molds were employed, and all measurements were carried out at room temperature (~25°C).

Density Functional Theory (DFT) Calculation: Calculation of the intercalation of two I^- and Cl^- ions into the interlayer of graphene/fluorinated graphene were performed within the framework of density functional theory (DFT) as implemented in the Vienna *Ab-initio* Simulation Package (VASP) code by using the projector augmented wave method with the Perdew-Burke-Ernzerhof (PBE) exchange-correlation functional [1]-[3]. The influence of vdW interactions is considered by using a modified version of vdW-DF, referred to as "optB86b-vdW" [4] [5]. The projector augmented wave potentialswere used with an energy cutoff of 500 Ev [6]. First, four-layer graphene/fluorinated graphene structure was fully optimized. A 9×9×1

Monkhorst-Pack method *k*-mesh was used for geometry optimization. Energy convergence of 1.0×10^{-4} meV $atom^{-1}$ was ensured during the self-consistent field calculations. And the convergence criteria for the atomic forces was 0.01 eV $Å^{-1}$. Next, two I^- and Cl^- were intercalated into graphene/fluorinated graphene, followed by structure optimization. There exists a vacuum layer of large than 20 Å perpendicular to the surface plane to isolate the mirror interactions. Further, single point energy calculation was performed. The charge density difference $\Delta\rho$ was calculated according to the following equation:

$$\Delta\rho = \rho_{total} - \rho_{cluster} - \rho_{slab}$$

Where ρ_{total} is the total charge density of the adsorption system, $\rho_{cluster}$ and ρ_{slab} are the charge densities of F_4ICl and F_4ICl_2 cluster, and graphene/fluorinated graphene slab, respectively. The charge density differences were visualized by VESTA. The cohesive energy of F_4ICl and F_4ICl_2 cluster intercalated into graphene/fluorinated graphene slab with four layers were calculated according to the following equation:

$$E_{CE} = E_{top\ layer\ graphene} + E_{other\ layers} + E_{cluster} - E_{total}$$

Where E_{CE} is the cohesive energy, $E_{total,}$ $E_{top\ layer\ graphene,}$ $E_{other\ layers}$ and $E_{cluster}$ are the energies of the entire structure, topmost layer graphene, other layers of graphene/fluorinated graphene excluded the top layer graphene, and F_4ICl and F_4ICl_2 cluster, respectively.

References

[1]. G. Kresse, J. Furthmuller, Efficient iterative schemes for ab initio total-energy calculations using a plane-wave basis set, Physical review B, 1996, 54(16): 11169-11186.

[2]. P.E. Blochl, Projector augmented-wave method, Physical review B, 1994, 50(24): 17953-17979.

[3]. J.P. Perdew, K. Burke, M. Ernzerhof, Generalized gradient approximation made simple, Physical review letters, 1996, 77(18): 3865-3868.

[4]. J. Klimes, D.R. Bowler, A. Michaelides, Chemical accuracy for the van der Waals density functional, Journal of Physics: Condensed Matter, 2009, 22(2): 022201.

[5]. J. Klimes, D.R. Bowler, A. Michaelides, Van der Waals density functionals applied to solids, Physical Review B—Condensed Matter and Materials Physics, 2011, 83(19): 195131.

[6]. G. Kresse, D. Joubert, From ultrasoft pseudopotentials to the projector augmented-wave method. Physical review B, 1999, 59(3): 1758–1775.

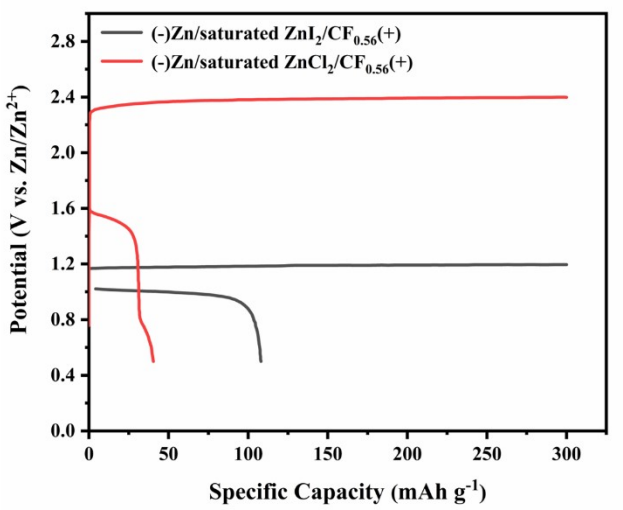

Figure S1. GCD curves of $CF_{0.56}$ electrode in the electrolyte solutions of ZnI_2-WISE and $ZnCl_2$-WISE under 0.75 A g^{-1}.

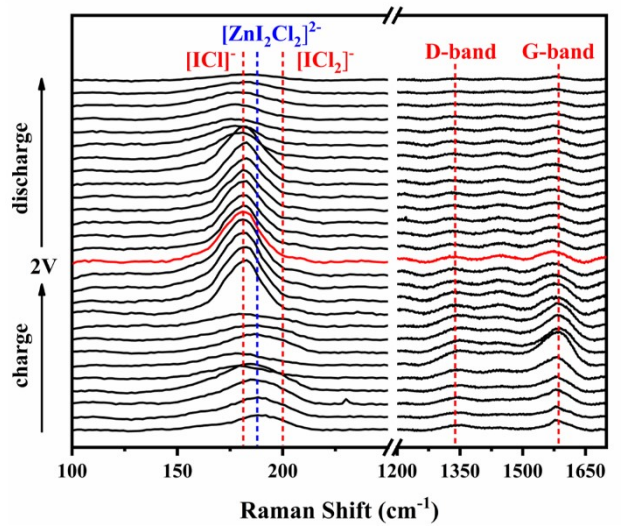

Figure S2. *In-situ* Raman spectra of NG electrode in 3 m ZnI_2 + 27 m $ZnCl_2$ electrolyte.

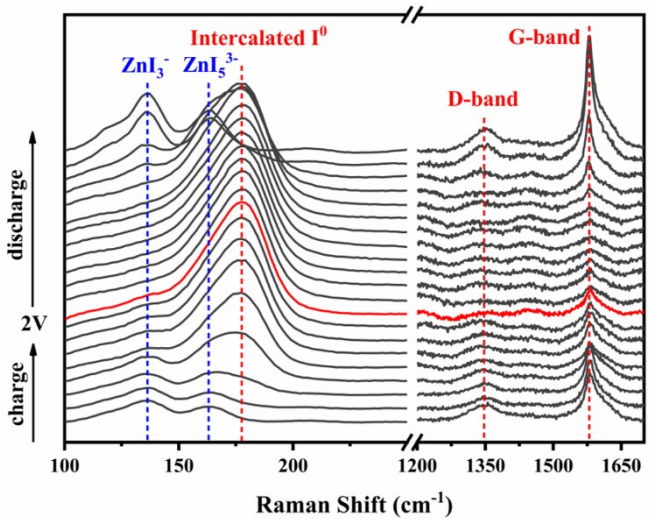

Figure S3. *In-situ* Raman spectra of NG electrode in ZnI_2-WISE.

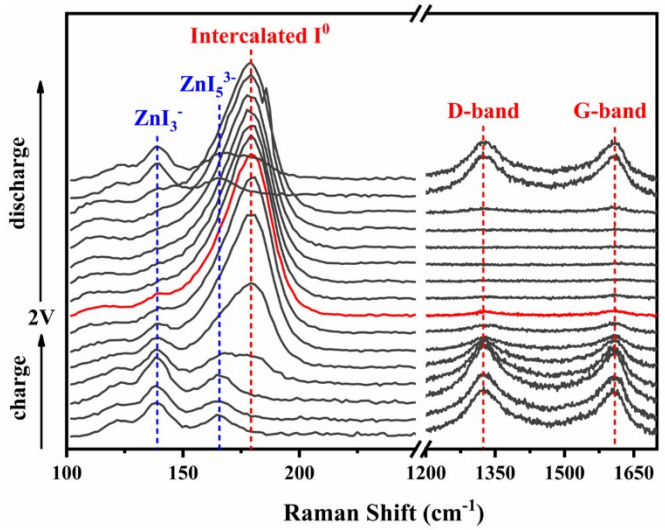

Figure S4. *In-situ* Raman spectra of $CF_{0.56}$ electrode in ZnI_2-WISE.

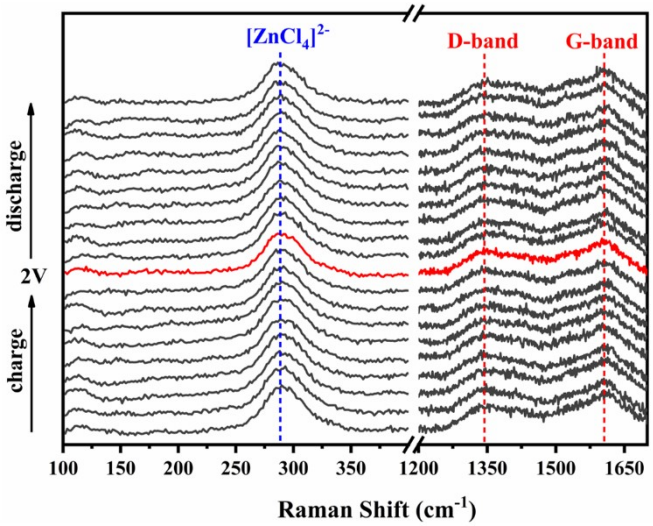

Figure S5. *In-situ* Raman spectra of $CF_{0.56}$ electrode in $ZnCl_2$-WISE.

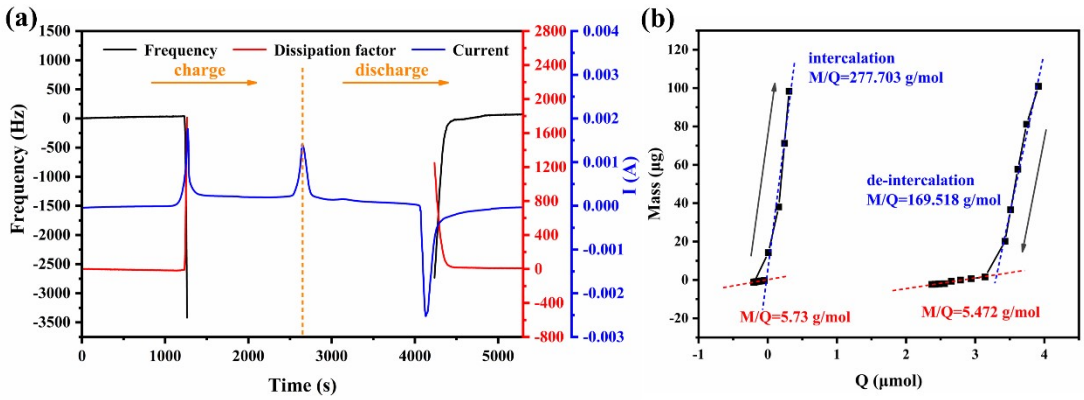

Figure S6. (a) CV-QCM curves of NG electrode during the battery operation. **(b)** Mass-charge relationships of NG electrode during the initial anion intercalation and the final anion de-intercalation processes.

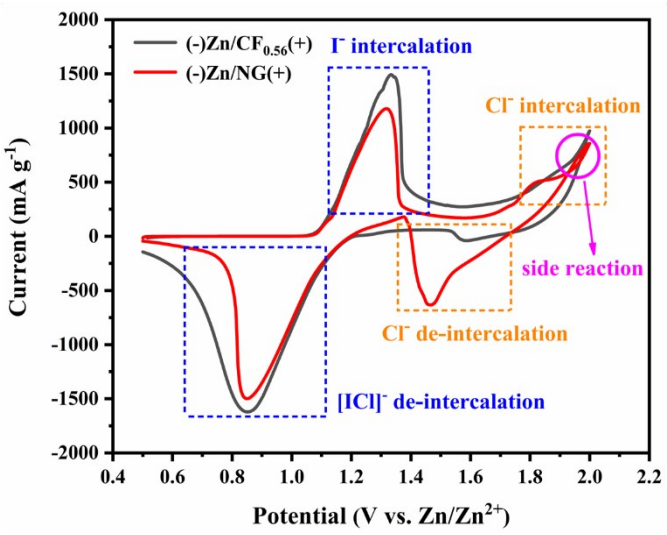

Figure S7. CV curves of NG and $CF_{0.56}$ electrodes under 0.5 mV s^{-1}.

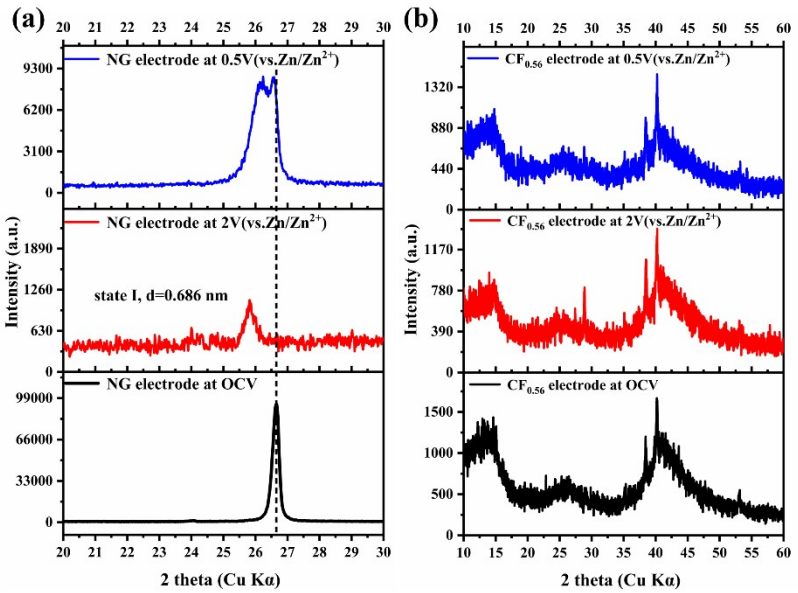

Figure S8. XRD patterns of **(a)** NG and **(b)** $CF_{0.56}$ electrodes at the OCV, fully charged and fully discharged states.

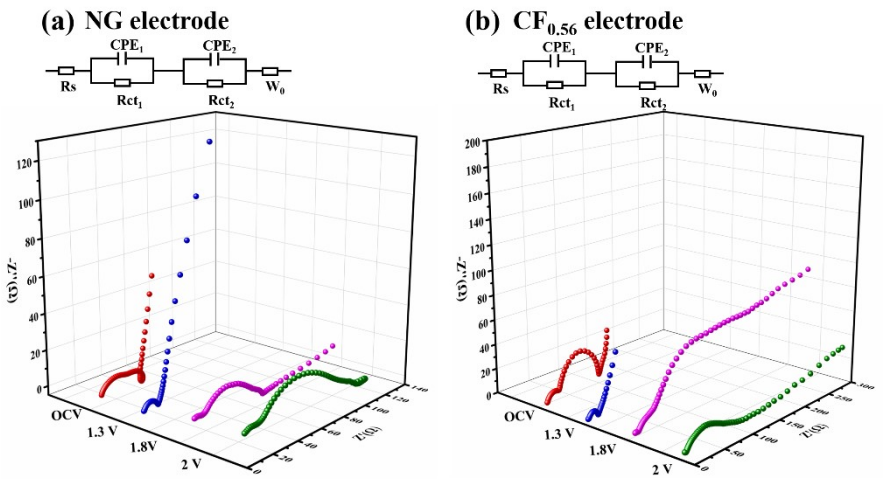

Figure S9. EIS results of **(a)** NG and **(b)** $CF_{0.56}$ electrodes in the electrolyte solutions of 3 m ZnI_2 + 27 m $ZnCl_2$ during the charge process.

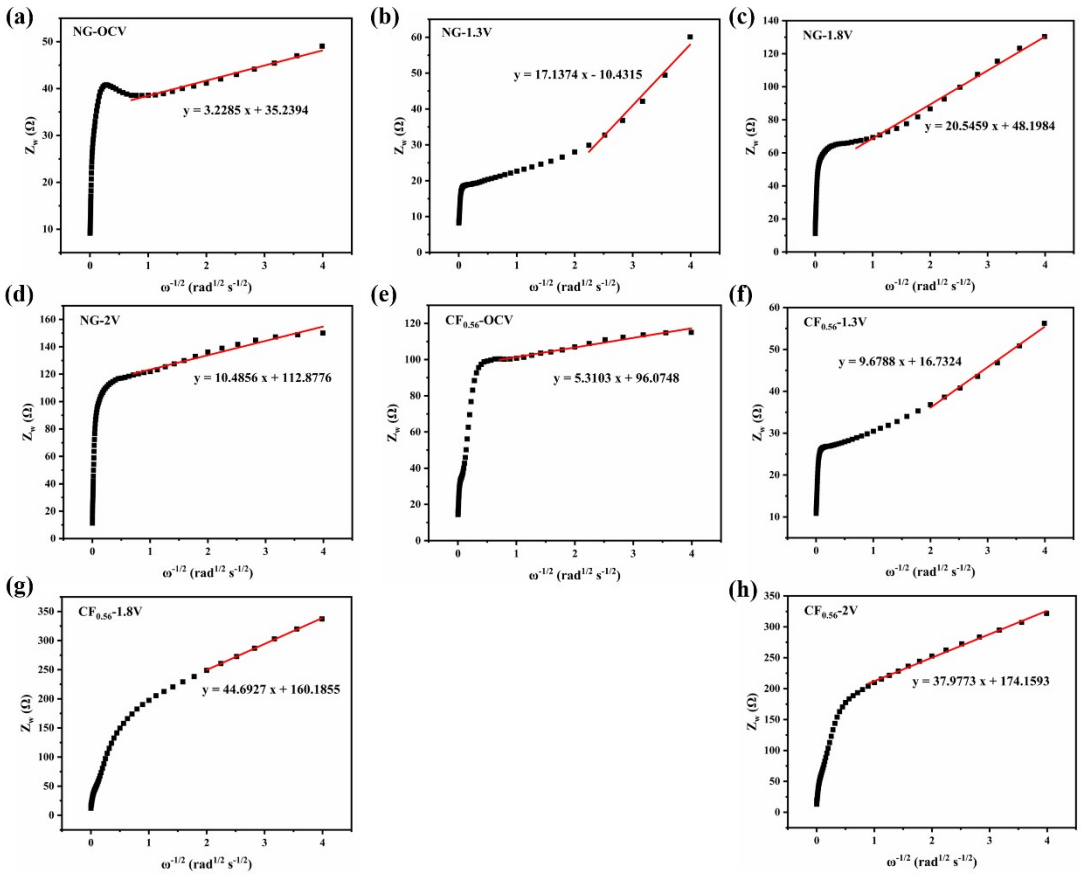

Figure S10. The Warburg impedances of NG and $CF_{0.56}$ electrodes at **(a, e)** OCV, **(b, f)** 1.3 V, **(c, g)** 1.8 V and **(d, h)** 2 V (vs. Zn/Zn^{2+}).

Table S1. The calculated results of NG and $CF_{0.56}$ electrodes basing on Warburg impedances.

Potential (V vs. Zn/Zn^{2+})		OCV	1.3 V	1.8 V	2 V
$CF_{0.56}$ electrode	σ ($\Omega\ s^{-1/2}$)	5.31	9.68	44.69	37.98
	dE/dQ ($V\ mol^{-1}$)	0	0.28	1.01	0.63
	D_{anion} ($*10^{-10}\ cm^2\ s^{-1}$)	0	7.27	4.57	2.45
NG electrode	σ ($\Omega\ s^{-1/2}$)	3.23	17.14	20.55	10.49
	dE/dQ ($V\ mol^{-1}$)	0	0.19	0.99	0.38
	D_{anion} ($*10^{-10}\ cm^2\ s^{-1}$)	0	0.41	7.41	4.14

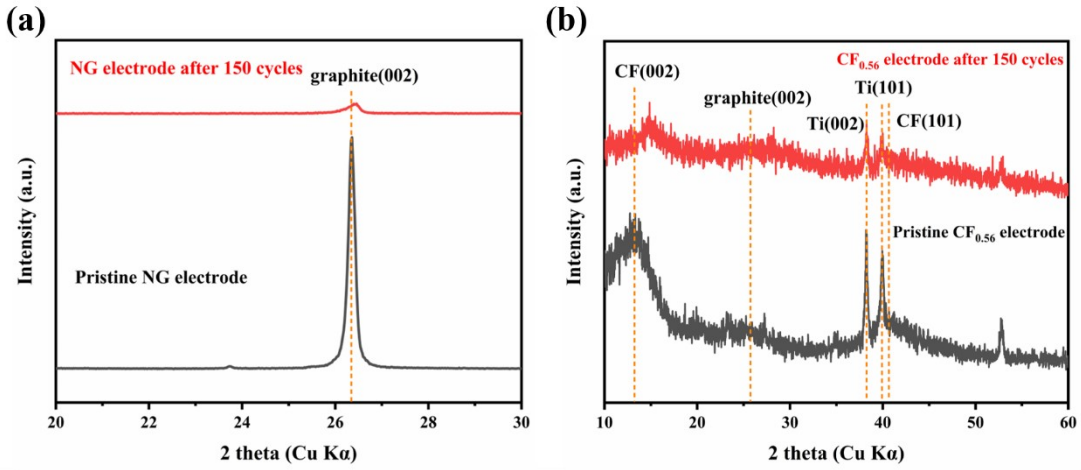

Figure S11. XRD patterns of **(a)** NG and **(b)** $CF_{0.56}$ electrodes before and after 150 cycles.

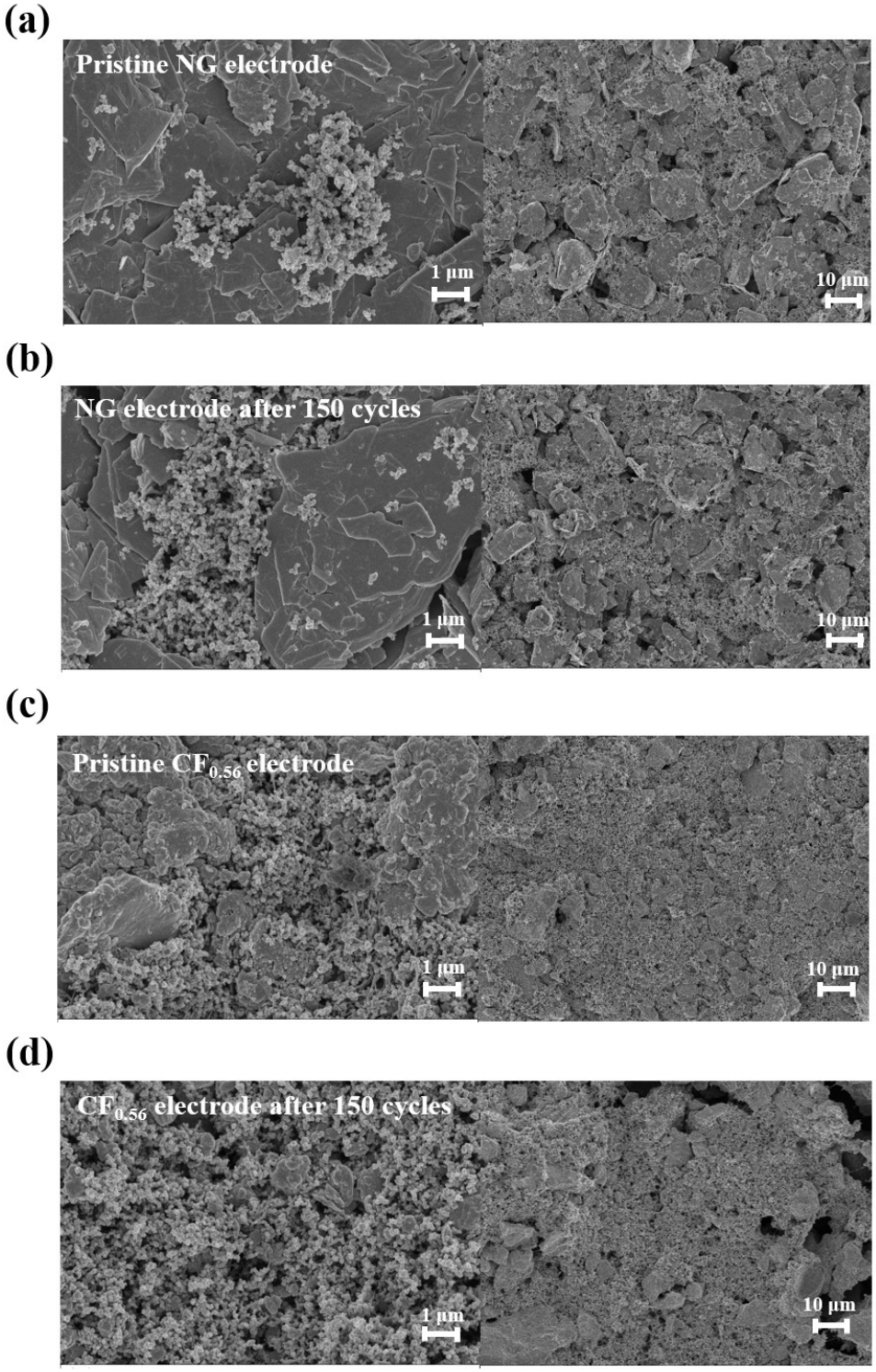

Figure S12. SEM images of **(a, b)** NG and **(c, d)** $CF_{0.56}$ electrodes before and after 150 cycles.

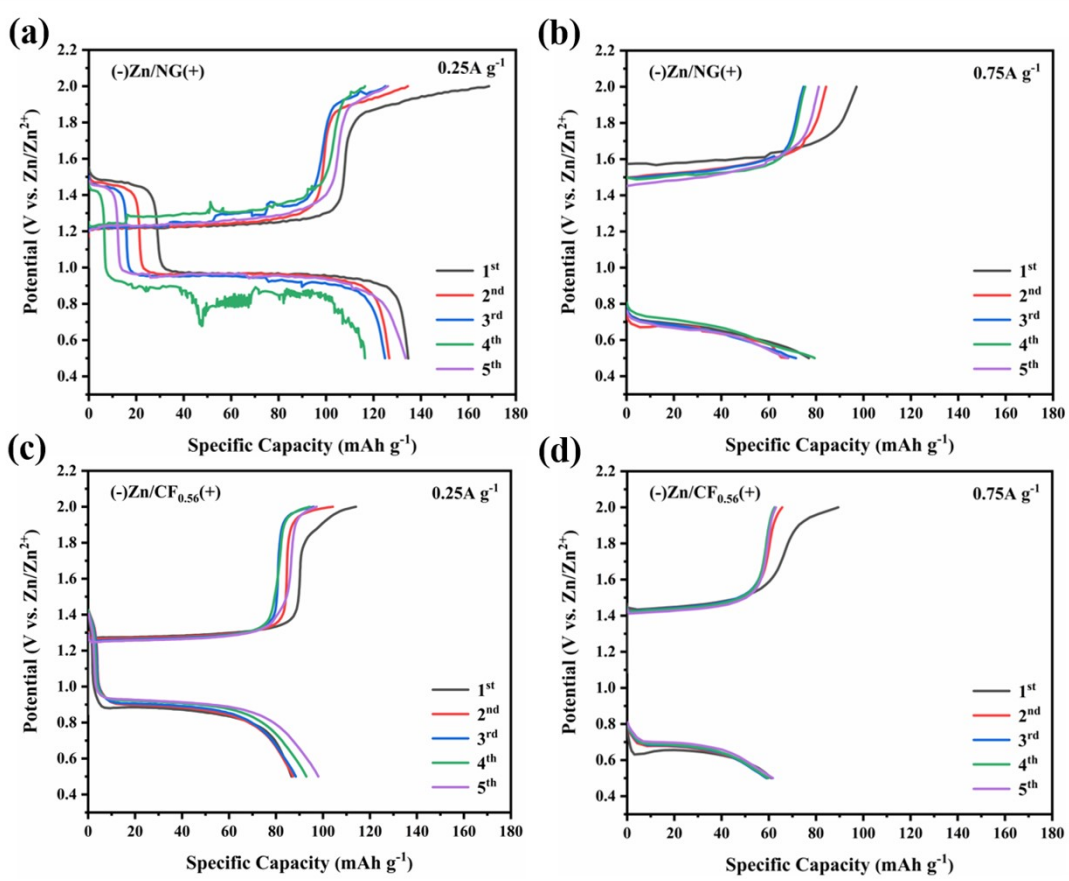

Figure S13. GCD curves **(a, b)** NG and **(c, d)** $CF_{0.56}$ electrodes at 0℃ using the WISE of 3 m ZnI_2 + 27 m $ZnCl_2$.

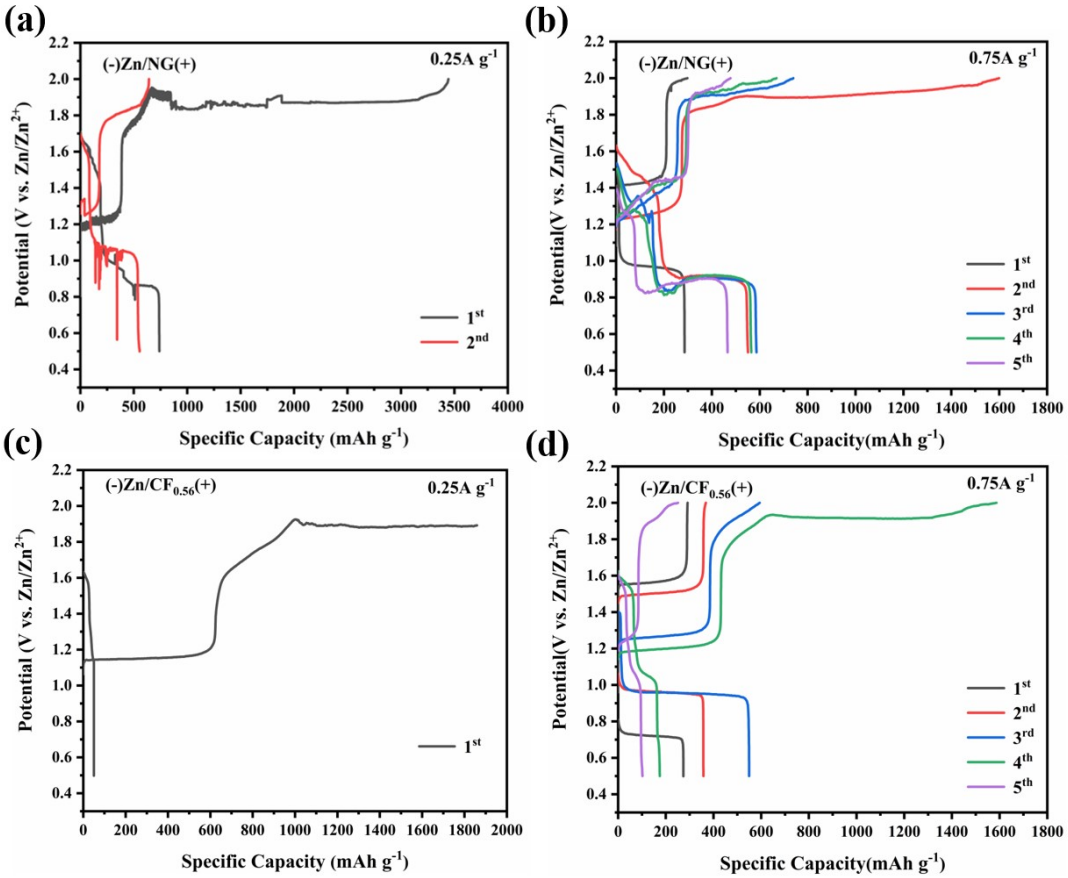

Figure S14. GCD curves **(a, b)** NG and **(c, d)** $CF_{0.56}$ electrodes at 50°C using the WISE of 3 m ZnI_2 + 27 m $ZnCl_2$.